Electronic Supplementary Material (ESI) for Green Chemistry.
This journal is © The Royal Society of Chemistry 2016

Electronic Supplementary Information

Hierarchical hollow nanostructured core@shell recyclable catalysts γ-Fe_2O_3@LDH@Au_{25}-*x* for highly efficient alcohol oxidation

Shuangtao Yin, Jin Li, and Hui Zhang*

State Key Laboratory of Chemical Resource Engineering, Beijing University of Chemical Technology, Beijing 100029, P. R. China.

*E-mail: huizhang67@gst21.com;

Fax: +8610-6442 5385;

Tel:+8610-6442 5872

TG, ESI-MS, ICP and BET Characterizations

The thermogravimetric analysis (TG) was performed on a Mettler-Toledo TGA/DSC 1/1100 ST thermal analyzer. Electrospray ionization mass spectra (ESI-MS) were recorded using a Waters Xevo G2S quadrupole time-of-flight (Q-TOF) mass spectrometer. The sample was dispersed in methanol and infused at a flow rate of 5 μL/min. The capillary voltage was set as 2.50 kV. The source temperature and desolvation temperature were 120 and 500 ^{o}C, respectively. The desolvation gas flow was 800 L/h. Elemental analysis for metal ions was done on a Shimadzu ICPS-7500 inductively coupled plasma atomic emission spectroscopy (ICP-AES) after dissolving sample in chloroazotic acid (1 mL) followed diluted to 10 mL using deionized water. Fourier transform infrared spectra (FT-IR) were obtained on a Bruker Vector-22 FT-IR spectro-photometer using KBr pellet technique (sample/KBr = 1/100). The specific surface area of Fe_3O_4 was determined by Brunauer-Emmett-Teller (BET) method from low temperature N_2 adsorption isotherm at 77 K on a Quantachrome Autosorb-1C-VP system.

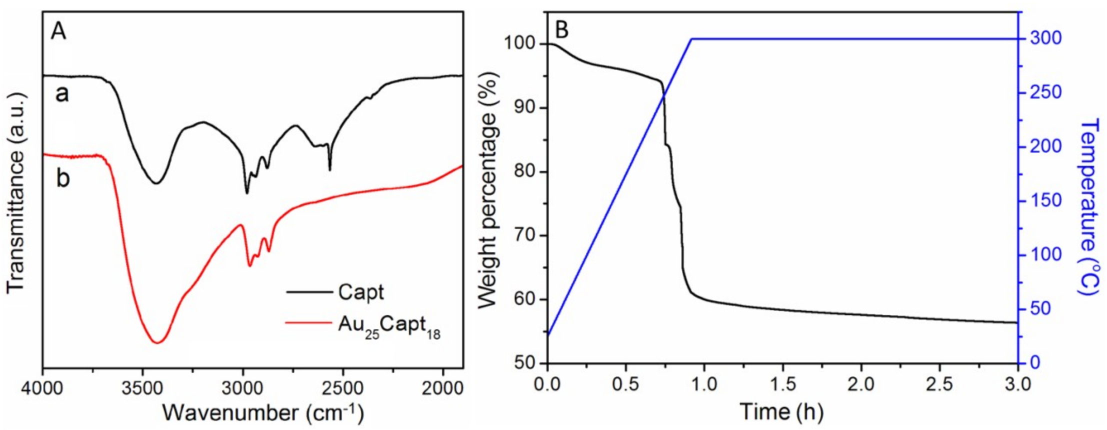

Fig. S1 FT-IR spectra (A) of Captopril (a) and $Au_{25}Capt_{18}$ (b), and TG analysis (B) of $Au_{25}Capt_{18}$.

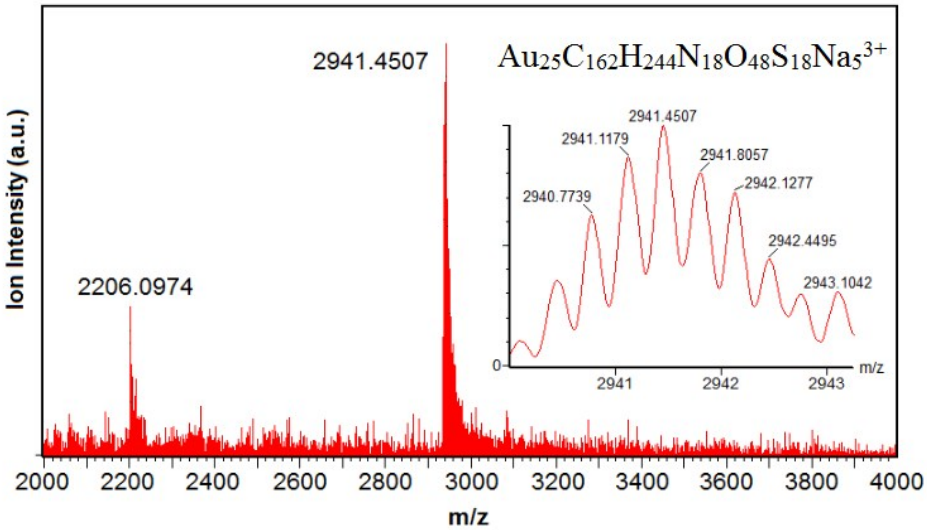

Fig. S2 Negative mode ESI-MS analysis and isotopically resolved spectra of $Au_{25}Capt_{18}$.

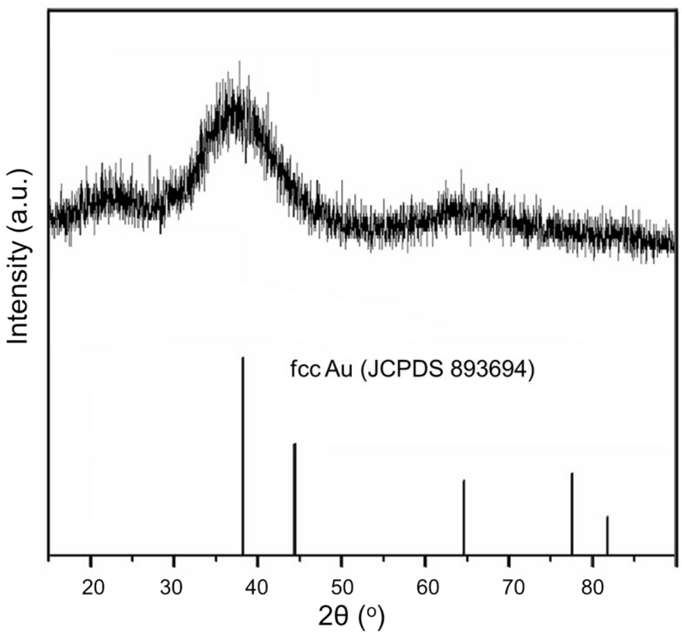

Fig. S3 The XRD pattern of $Au_{25}Capt_{18}$

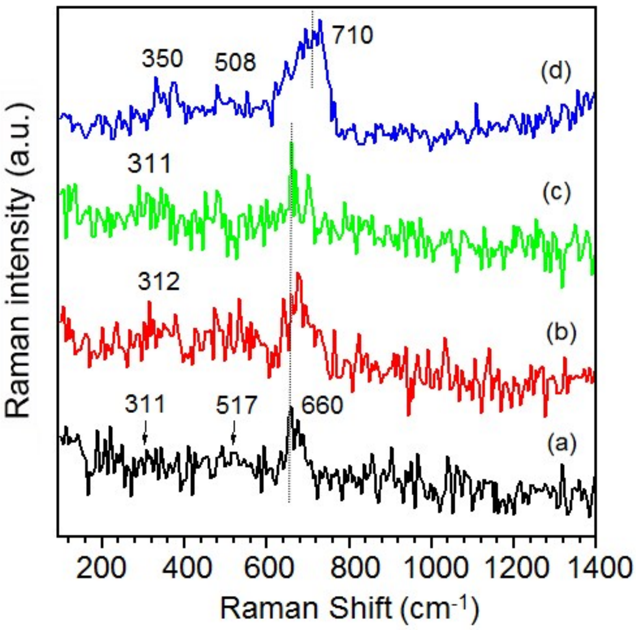

Fig. S4 Raman spectra of the pure Fe_3O_4 core (a), the magnetic support Fe_3O_4@Ni_3Al-LDH (b), the catalyst precursor Fe_3O_4@Ni_3Al-LDH@$Au_{25}Capt_{18}$-0.053 (c) and the catalyst γ-Fe_2O_3@Ni_3Al-LDH@Au_{25}-0.053 (d).

Fig. S4 presents a series of samples including the catalyst γ-Fe_2O_3@Ni_3Al-LDH@Au_{25}-0.053, corresponding support Fe_3O_4@Ni_3Al-LDH and precursor Fe_3O_4@Ni_3Al-LDH@$Au_{25}Capt_{18}$-0.053, and Fe_3O_4 core. Clearly, the pure Fe_3O_4 core exhibits a main strong band centered at 660 cm^{-1} and two low strength ones at 517 and 311 cm^{-1}, which are characteristics of pure magnetite phase (T. Fan and H. Zhang et al., *Ind. Eng. Chem. Res.*, 2011, **50**, 9009). Then the support Fe_3O_4@Ni_3Al-LDH and the catalyst precursor Fe_3O_4@Ni_3Al-LDH@$Au_{25}Capt_{18}$-0.053 show the similar characteristics to Fe_3O_4, indicating the existence of the main Fe_3O_4 phase in these two samples. However, the catalyst γ-Fe_2O_3@Ni_3Al-LDH@Au_{25}-0.053 exhibits three broad structures at ca. 350, 508, and 710 cm^{-1}, which are typical characteristics of the maghemite (D. L. A. de Faria. et al., J. Raman Spectrosc. 1997, 28, 873), clearly indicating the occurrence of phase transformation from Fe_3O_4 to γ-Fe_2O_3 in the catalyst upon the loading of $Au_{25}Capt_{18}$ and calcinations.

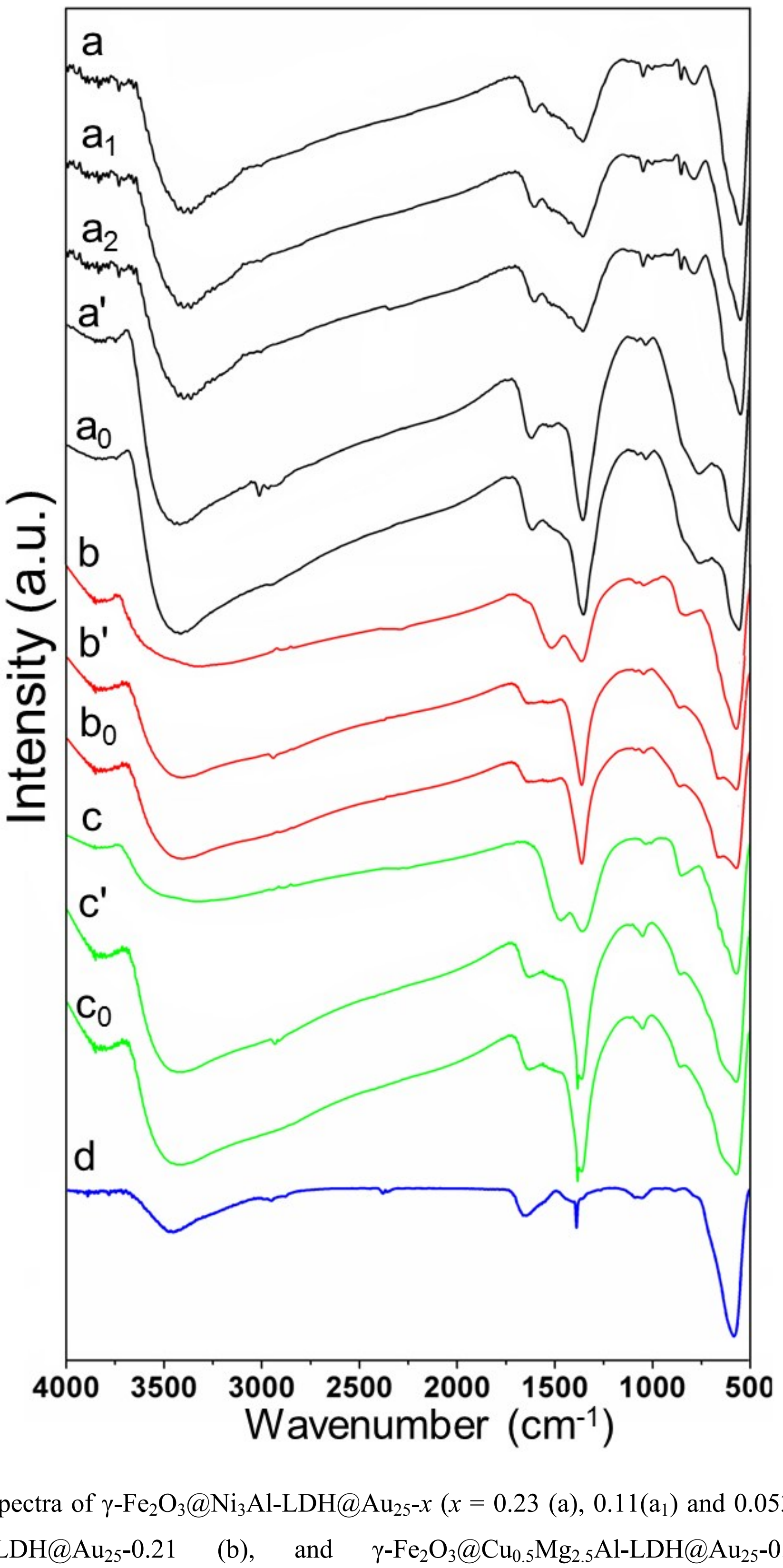

Fig. S5 FT-IR spectra of γ-Fe_2O_3@Ni_3Al-LDH@Au_{25}-x (x = 0.23 (a), 0.11(a_1) and 0.053 (a_2), γ-Fe_2O_3@Mg_3Al-LDH@Au_{25}-0.21 (b), and γ-Fe_2O_3@$Cu_{0.5}Mg_{2.5}Al$-LDH@Au_{25}-0.2 (c), corresponding precursors (a'-c') and supports (a_0-c_0) and Fe_3O_4 (d).

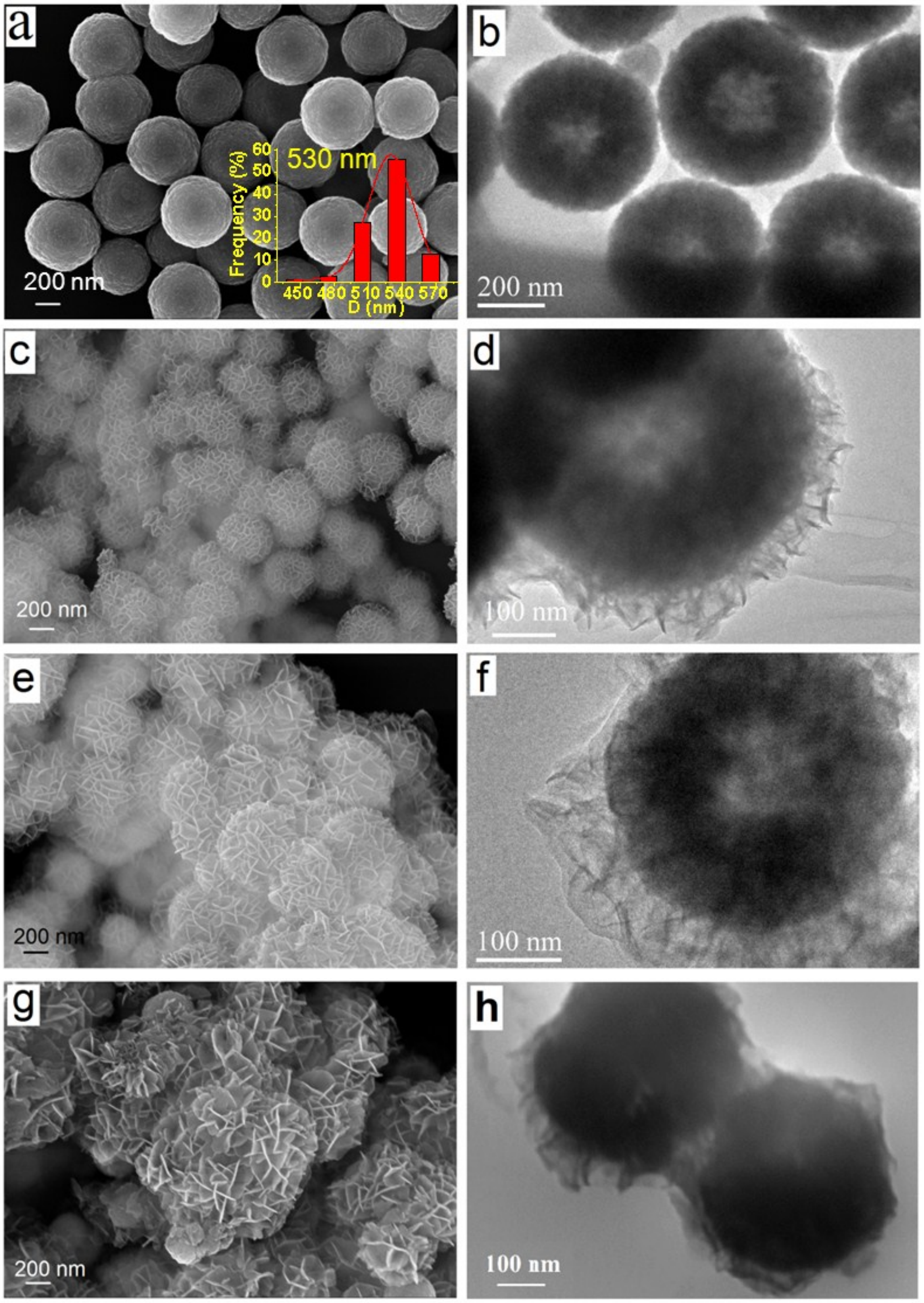

Fig. S6 SEM (a, c, d, g) and TEM (b, d, f, h) images of Fe_3O_4 (a, b) and magnetic supports Fe_3O_4@Ni_3Al-LDH(c, d), Fe_3O_4@Mg_3Al-LDH (e, f) and Fe_3O_4@$Cu_{0.5}Mg_{2.5}$Al-LDH (g, h).

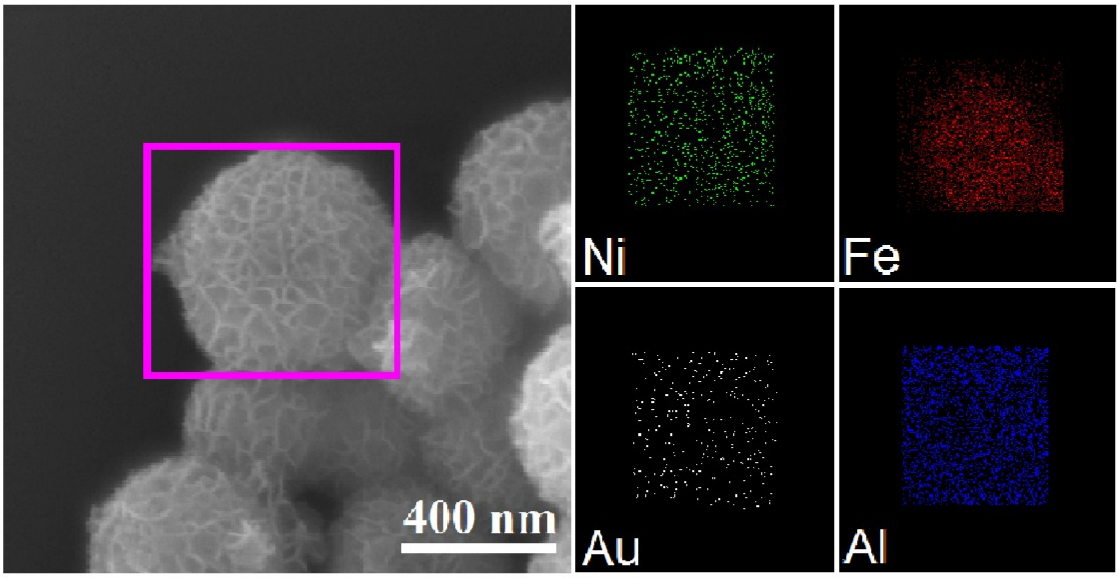

Fig. S7 SEM and element mapping images of γ-Fe_2O_3@Ni_3Al-LDH@Au_{25}-0.053.

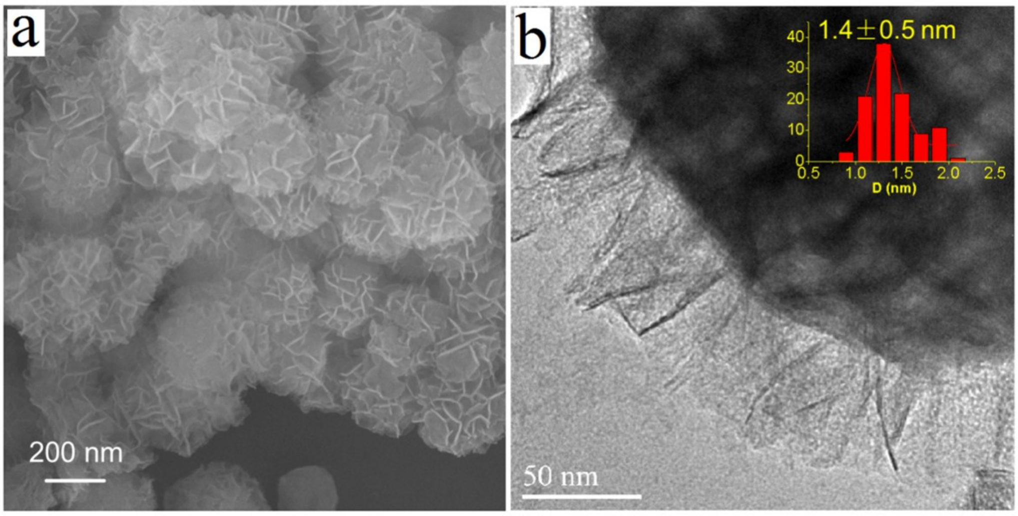

Fig. S8 SEM (a) and HRTEM (b) images of recovered catalyst γ-Fe_2O_3@Ni_3Al-LDH@Au_{25}-0.053 after ten runs (inset: the histogram of the size distribution).

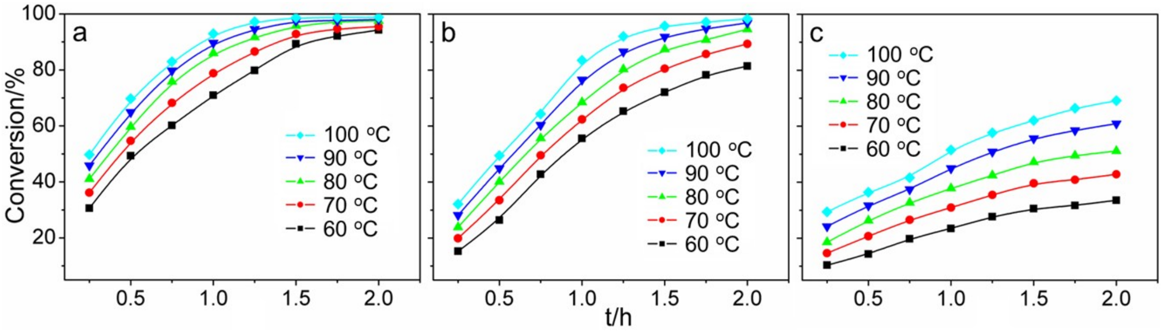

Fig. S9 Conversion-time (t) plots for the aerobic oxidation of 1-phenylethanol over γ-Fe_2O_3@Ni_3Al-LDH@Au_{25}-0.23 (a), γ-Fe_2O_3@Mg_3Al-LDH@Au_{25}-0.21 (b), and γ-Fe_2O_3@$Cu_{0.5}Mg_{2.5}Al$-LDH@Au_{25}-0.2 at various reaction temperature in toluene.

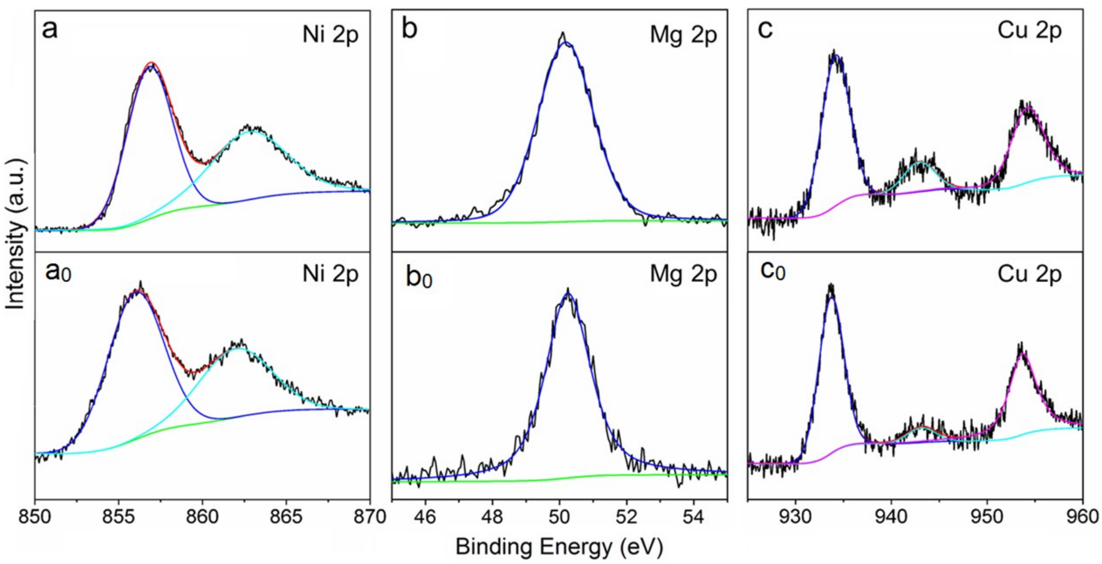

Fig. S10 M 2p (M=Ni, Mg, Cu) XPS of γ-Fe_2O_3@Ni_3Al-LDH@Au_{25}-0.23 (a), γ-Fe_2O_3@Mg_3Al-LDH@Au_{25}-0.21 (b), γ-Fe_2O_3@$Cu_{0.5}Mg_{2.5}Al$-LDH@Au_{25}-0.2 (c) and the supports (a_0-c_0).

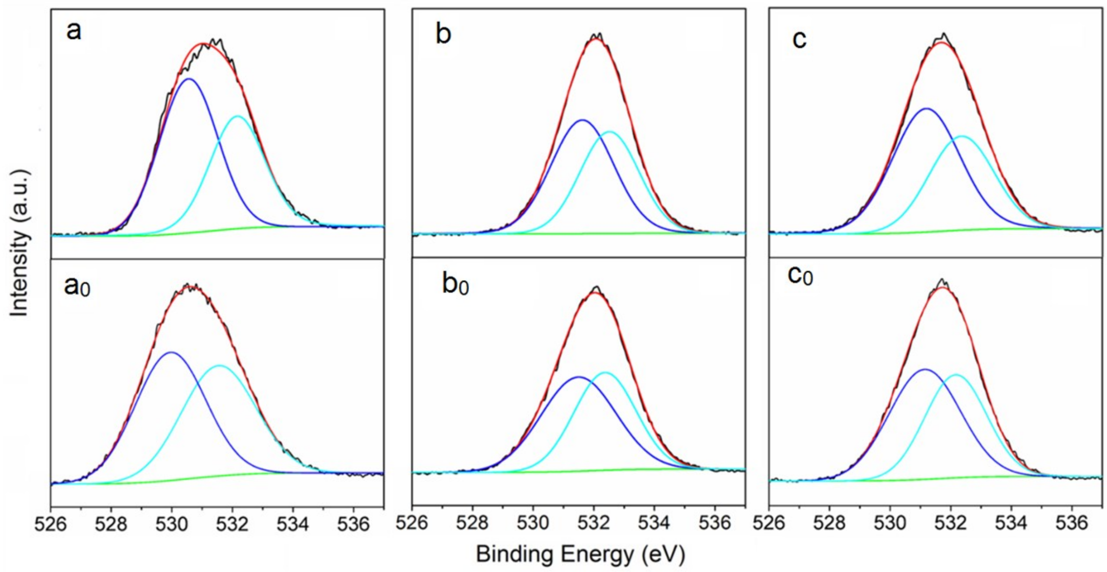

Fig. S11 O1s XPS spectra of γ-Fe_2O_3@Ni_3Al-LDH@Au_{25}-0.23 (a), γ-Fe_2O_3@Mg_3Al-LDH@Au_{25}-0.21 (b), γ-Fe_2O_3@$Cu_{0.5}Mg_{2.5}$Al-LDH@Au_{25}-0.2 (c), and corresponding supports (a_0-c_0).

Table S1 XRD parameters of the catalysts γ-Fe_2O_3@M_3Al-LDH@Au_{25}-*x*, corresponding supports Fe_3O_4@M_3Al-LDHs and Fe_3O_4 core.

Samples	d_{003} /nm	d_{110} /nm	a /nm[a]	c /nm[a]	D_{003} /nm[b]	D_{110} /nm[b]	d_{311} /nm	a /nm[c]	D_{311} /nm[b]
Fe_3O_4	-	-	-	-	-	-	0.2530	0.839	29.6
Fe_3O_4@Ni_3Al-LDH	0.7519	0.1503	0.3006	2.25	11.4	76.2	0.2524	0.837	28.2
Fe_3O_4@Mg_3Al-LDH	0.7769	0.1506	0.3012	2.33	15.4	91.1	0.2533	0.840	28.8
Fe_3O_4@$Cu_{0.5}Mg_{2.5}$Al-LDH	0.7541	0.1497	0.2994	2.26	18.4	91.8	0.2502	0.830	28.7
γ-Fe_2O_3@Ni_3Al-LDH@Au_{25}-0.23	0.6782	0.1502	0.3004	2.03	10.3	71.1	0.2513	0.833	25.8
γ-Fe_2O_3@Ni_3Al-LDH@Au_{25}-0.11	0.683	0.150	0.300	2.05	10.5	72.2	0.253	0.83	25.9

	4	3	6				1	9	
γ-Fe_2O_3@Ni_3Al-LDH@Au_{25}-0.053	0.6827	0.1501	0.3002	2.05	10.4	72.5	0.2527	0.838	25.8
γ-Fe_2O_3@Mg_3Al-LDH@Au_{25}-0.21	0.6643	0.1504	0.3008	1.99	12.6	77.3	0.2516	0.834	24.8
γ-Fe_2O_3@$Cu_{0.5}Mg_{2.5}$Al-LDH@Au_{25}-0.2	0.6638	0.1498	0.2996	1.99	11.75	80.2	0.2496	0.828	24.3

[a] Based on hexagonal crystal system, $a = 2d_{110}$, $c = 3d_{003}$. [b] Calculated by Scherrer formula, $D_{hkl} = K\lambda/(\beta\cos\theta)$ (K = 0.89; λ is the X-ray wavelength (0.1542 nm), θ is Bragg diffraction angle, β is the full width at half-maximum (in radian)). [c] Based on cubic crystal system, $1/d_{hkl}^2 = (h^2+k^2+l^2)/a^2$.

Table S2 Chemical compositions of the γ-Fe_2O_3@M_3Al-LDH@Au_{25}-*x* catalysts by ICP analysis.

Catalysts	Au (wt%)	Ni (wt%)	Mg (wt%)	Cu (wt%)	Al (wt%)	M(=Ni, Mg, CuMg)/Al molar ratio	Fe (wt%)
γ-Fe_2O_3@Ni_3Al-LDH@Au_{25}-0.23	0.23	30.81	-	-	4.87	2.909	35.67
γ-Fe_2O_3@Ni_3Al-LDH@Au_{25}-0.11	0.11	30.74	-	-	4.85	2.915	34.95
γ-Fe_2O_3@Ni_3Al-LDH@Au_{25}-0.053	0.053	32.15	-	-	5.08	2.911	35.89
γ-Fe_2O_3@Mg_3Al-LDH@Au_{25}-0.21	0.21	-	11.67	-	4.56	2.879	32.15
γ-Fe_2O_3@$Cu_{0.5}Mg_{2.5}$Al-LDH@Au_{25}-0.2	0.20	-	8.96	4.73	4.53	2.671	33.59

Table S3 Kinetic fitting of the aerobic oxidation of 1-phenylethanol reaction over the catalysts.[a]

Catalysts	T (K)	k (h^{-1}) [b]	R^2	E_a (kJ/mol) [c]	R^2
γ-Fe_2O_3@Ni_3Al-LDH@Au_{25}-0.23	333.15	1.422	0.9696	19.15	0.9989
	343.15	1.7122	0.9865		
	353.15	2.1055	0.9939		
	363.15	2.4734	0.9919		
	373.15	2.9886	0.9877		
γ-Fe_2O_3@Mg_3Al-LDH@Au_{25}-0.21	333.15	0.9104	0.9965	23.35	0.9978
	343.15	1.1915	0.9963		
	353.15	1.5300	0.9906		
	363.15	1.8486	0.9923		
	373.15	2.2576	0.9876		

γ-Fe_2O_3@$Cu_{0.5}Mg_{2.5}Al$-LDH@Au_{25}-0.2	333.15	0.1770	0.9741	26.66	0.9993
	343.15	0.2346	0.9773		
	353.15	0.2988	0.9822		
	363.15	0.3943	0.9907		
	373.15	0.4959	0.9931		

[a] Reaction condition: 1-phenylethanol (1 mmol), catalyst (Au: 0.2 mol%), toluene (5 mL), O_2 (20 mL/min), temperatures (60, 70, 80, 90, and 100 ^{o}C). [b] According to equation: ln (C_t/C_0) = - kt (C_t is the concentration of 1-phenylethanol at t time, mol/L; C_0 is the initial concentration of 1-phenylethanol, mol/L; k is the reaction rate constant, h^{-1}; and t is the reaction time, h). [c] According to Arrhenius equation: $\ln k = \ln A - E_a/RT$ (E_a is the apparent activation energy, kJ·mol^{-1}, k is the reaction rate constant, h^{-1}, A is the pre-exponential factor, h^{-1}; R is the molar gas constant, 8.314 J·mol^{-1}·K^{-1}, and T is the absolute temperature, K).

Table S4 XPS data of the γ-Fe_2O_3@M_3Al-LDH@Au_{25}-x catalysts compared with corresponding supports and Fe_3O_4 core

Samples	Fe 2p3/2 (eV)		M 2p3 (eV)	O 1s (eV)	
	Fe^{3+}	Fe^{2+}	Ni/Mg/Cu	(-OH)	(O^{2-})
γ-Fe_2O_3@Ni_3Al-LDH@Au_{25}-0.23	711.9	-	856.8	532.1 (45.1%)	530.5 (54.9%)
Fe_3O_4@Ni_3Al-LDH	712.8	710.5	856.0	531.5 (47.6%)	529.9 (52.4%)
γ-Fe_2O_3@Mg_3Al-LDH@Au_{25}-0.21	711.3	-	50.1	532.5 (42.1%)	531.6(57.9%)
Fe_3O_4@Mg_3Al-LDH	711.8	710.7	50.2	532.4 (46.2%)	531.5(53.8%)
γ-Fe_2O_3@$Cu_{0.5}Mg_{2.5}$Al-LDH@Au_{25}-0.2	711.4	-	934.1	532.3 (41.3%)	531.2 (58.7%)
Fe_3O_4@$Cu_{0.5}Mg_{2.5}$Al-LDH	712.1	710.6	933.6	532.1 (44.7%)	531.1 (55.3%)
Fe_3O_4	711.4	710.4	-	531.1 (50.8%)	530.0 (49.2%)